T-Shaped 8-Aryl(ethynyl)-Substituted Psoralens With Tunable Charge-Transfer Absorption

Lena T. Leusch, Thomas J. J. Müller

European Journal of Organic Chemistry

EurJOC
European Journal of Organic Chemistry

Chemistry Europe
European Chemical Societies Publishing

RESEARCH ARTICLE OPEN ACCESS

T-Shaped 8-Aryl(ethynyl)-Substituted Psoralens With Tunable Charge-Transfer Absorption

Lena T. Leusch | Thomas J. J. Müller

Institut für Organische Chemie und Makromolekulare Chemie, Heinrich-Heine-Universität Düsseldorf, Düsseldorf, Germany

Correspondence: Thomas J. J. Müller (ThomasJJ.Mueller@hhu.de)

Received: 18 November 2025 | **Revised:** 12 December 2025 | **Accepted:** 29 December 2025

Keywords: acidochromism | cross-coupling reactions | density functional theory calculations | donor–acceptor dyes | fluorescence | solvatochromism

ABSTRACT

Two series of novel T-shaped 8-substituted psoralen derivatives bearing (hetero)aryl and arylethynyl substituents were synthesized via Suzuki and Sonogashira coupling starting from 8-methoxypsoralen (8-MOP). Predominantly, electron-donating substituents such as anisyl and phenothiazine were introduced at the 8-position of the psoralen for increasing the electron density in comparison to 8-MOP. Photophysical properties were studied by absorption and emission spectroscopy in solution and in the solid state. Increasing the donor strength of the substituent causes a bathochromic shift of both absorption and emission maxima. The absorption behavior can be correlated with Hammett substituent parameters of remote substituents at the *p*-aryl moieties that are directly or by ethynyl spacing positioned at the 8-position of psoralen. In most cases, fluorescence in the solid state is more pronounced than in solution. One derivative also displays significant aggregation-induced emission. For two amino-substituted psoralen derivatives, positive emission solvatochromism was observed and associated with a considerable change of dipole moment upon photonic excitation according to Lippert–Mataga analysis. Furthermore, the pK_a value of the T-shaped dimethylaminophenyl psoralen derivative was determined from absorption spectra. In addition, emission quenching is caused by protonation on the nitrogen atom. TD-DFT (time-dependent density functional theory) calculations are in good agreement with experimental data and rationalize the electronic structure.

1 | Introduction

Psoralens, which occur naturally in the plant *Psoralea corylifolia* [1], have long been applied in traditional medicine [2] and remain clinically relevant for the treatment of skin diseases such as vitiligo [3, 4], psoriasis [5], and certain lymphomas [6, 7]. Well-known representatives in clinical application include 8-methoxypsoralen (8-MOP), 5-methoxypsoralen (5-MOP) and 4,5′,8-trimethylpsoralen (TMP) (Figure 1) [8]. In clinical PUVA (psoralen + UV-A light) therapy, psoralens are administered orally or topically [9]. The mode of action begins with intercalation of psoralen molecules into the DNA helix. Upon irradiation with UV light, they undergo photoinduced [2 + 2] cycloaddition, preferably with adjacent thymine bases [10], at the furan or pyrone double bonds of the psoralen molecule [11]. The formation of monoadducts and cross-links between the DNA strands leads to inhibition of DNA replication and thus leads into apoptosis [12]. In addition to this well-studied PUVA mechanism, recent studies have revealed competing photophysical pathways. For instance, a photoinduced electron transfer (PET) between guanine as an electron donor and psoralen as an electron acceptor in competition to the cycloaddition was reported by the Gilch group [13, 14]. Thus, exploring further synthetic pathways is essential to generate further psoralen derivatives whose photophysical and electronic properties can be tailored through suitable substituents. In particular, increasing the electron density of the psoralene scaffold beyond the one of 8-MOP should increase the HOMO level and thereby suppress the competing PET between guanine and the psoralene derivative in favor of [2 + 2] cycloaddition.

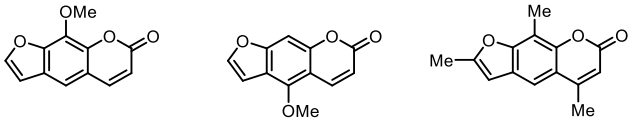

FIGURE 1 | Selected psoralen compounds.

We have previously established synthetic strategies for the derivatization of psoralen in the 5- and 8-positions by catalytic strategies and presented the photophysical and electronic characteristics of these psoralene cruciforms [15, 16]. Here, based on these results, we report the synthesis of predominantly novel T-shaped psoralen derivatives, predominantly with electron-donating substituents in 8-position, accessible from 8-methoxypsoralen in a few steps via various cross-coupling reactions. The photophysical properties were investigated in solution, in the solid state, and upon embedding in a PMMA matrix, including solvatochromism as well as effects of induced aggregation.

2 | Results and Discussion

2.1 | Synthesis

The synthetic strategy employs 8-methoxypsoralen (**1**) as a starting material. Demethylation to the phenol **2** with boron tribromide [17], followed by triflation using trifluoromethanesulfonic acid anhydride (**3**) [18] affords the target compound 8-triflato psoralen **4** in two steps with an overall yield of 71% (Scheme 1). This versatile precursor for subsequent cross-coupling reactions allows for efficient introduction of diverse substituents at 8-position.

Following previously reported conditions, triflate **4** undergoes Suzuki cross-coupling with various boronic acids and boronates **5** employing $Pd(dba)_2$ as a catalyst, Sphos as the ligand, and potassium phosphate as a base [16]. Both electron-deficient and electron-rich substituents can be successfully introduced, affording a total of eight 8-aryl-substituted psoralen derivatives **6** in moderate to excellent yields (Scheme 2).

The introduction of a phenothiazine moiety is achieved via a bromine–lithium exchange borylation-Suzuki (BLEBS) sequence starting from compound **7**, where the bromine atom of phenothiazine is initially replaced by lithium and subsequently transmetallated into the corresponding boronate [19]. Subsequent Suzuki conditions with triflate **4** give rise to the formation and isolation of compound **6i** in 80% yield in a one-pot fashion (Scheme 3).

In addition, various terminal alkynes **8** can be coupled to the 8-position of the psoralen core under Sonogashira conditions

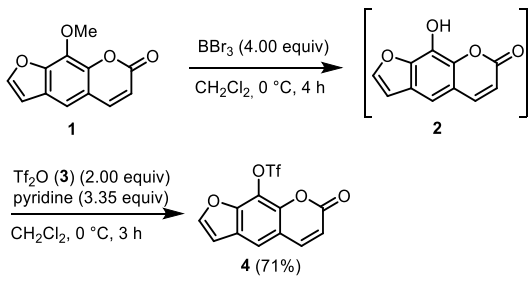

SCHEME 1 | Synthesis of 8-triflato psoralen **4**.

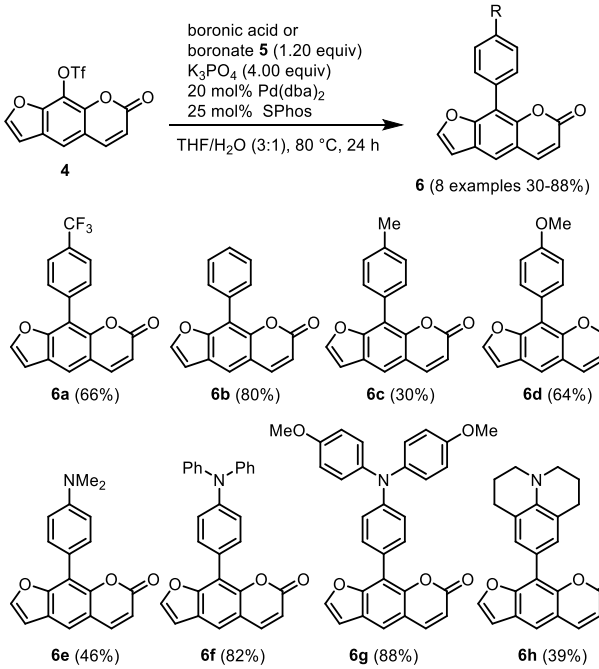

SCHEME 2 | Synthesis of 8-aryl-substituted psoralens **6** by Suzuki coupling.

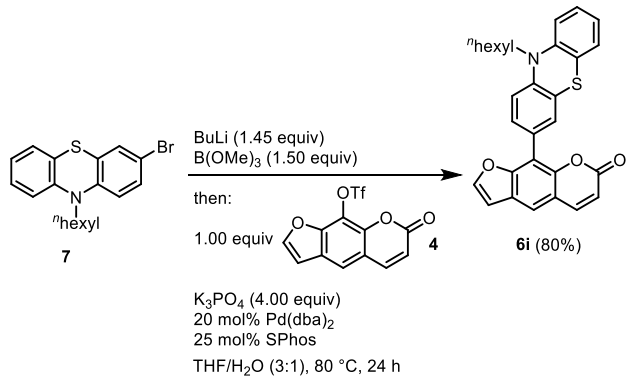

SCHEME 3 | One-pot BLEBS synthesis of phenothiazine-substituted psoralen **6i**.

employing $Pd(PPh_3)_4$ as catalyst and triethylamine as the base [16]. One example containing an electron-withdrawing group and four examples with electron-donating substituents of alkynylated derivatives **9** are obtained in good to excellent yields (Scheme 4).

The structure of the (hetero)aryl substituted psoralens **6** and arylethynyl-substituted psoralens **9** was unambiguously assigned via extensive NMR studies, mass spectrometry, and IR spectroscopy, and its molecular composition by combustion analysis or HRMS. As a representative example, the structure of derivative **6c** was elucidated by 2D NMR spectroscopy (see Supporting Information).

2.2 | Photophysical Properties

The photophysical properties of all derivatives **6** and **9** were investigated in dichloromethane solution and in the solid state.

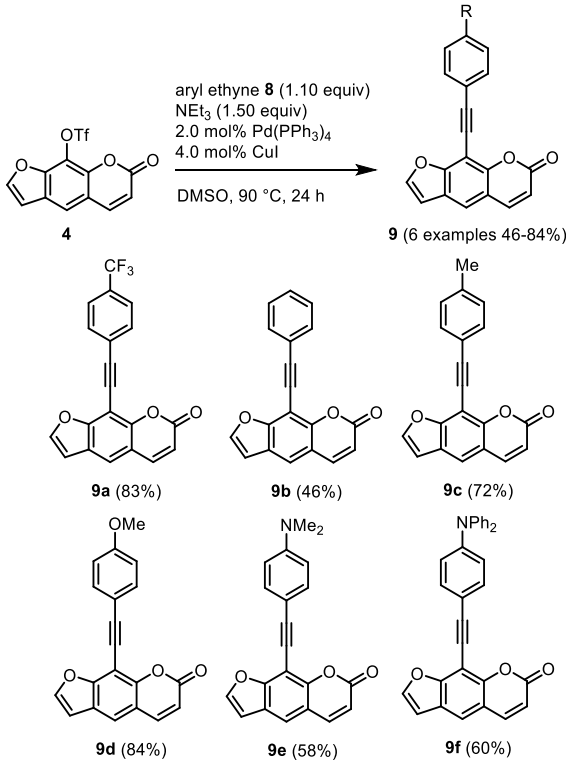

SCHEME 4 | Synthesis of 8-alkynyl-substituted psoralens **9** by Sonogashira coupling.

The aryl-substituted derivatives **6** exhibit intense absorption maxima between 271 and 303 nm with extinction coefficients ranging from 10 900 to 34 000 $M^{-1}\,cm^{-1}$. The longest wavelength absorption bands are predominantly observed as shoulders between 334 and 375 nm with extinction coefficients between 3100 and 12 900 $M^{-1}\,cm^{-1}$. A bathochromic shift of the longest-wavelength absorption maximum is observed with increasing donor strength of the substituents, a trend that becomes even more pronounced in the emission maxima, which appear in a range from 433 to 646 nm. The shift of the emission maximum from *p*-anisyl dye (**6d**) to *p*-(dimethylamino)phenyl dye (**6e**) accounts to 4700 cm^{-1}. This is consistent with previous findings on 5,8-diaryl-substituted psoralen cruciform dyes, where the change from *p*-anisyl to *p*-(dimethylamino)phenyl groups in the 8-position with identical substituents in 5-position leads to a bathochromic shift of the emission maxima by 4700–5300 cm^{-1} [16]. Thus, replacing the diphenylamino substituent (compound **6f**) with the dianisylamino group (compound **6g**) results in a further redshift of the emission maximum by 2400 cm^{-1} (Figure 2). In addition, this bathochromic shift by donor substitution for the series **6** is accompanied by an increase of the fluorescence quantum yield Φ_F in solution up to 0.07 for compound **6f**. However, in the solid state, the emission maxima of all dyes **6** are hypsochromically shifted. For most derivatives, the fluorescence quantum yield Φ_F is higher in the solid state than in solution, amounting up to 0.19 for dye **6h** (Table 1).

Likewise, the photophysical properties of 8-alkynyl-substituted derivatives **9** were investigated. Dyes **9** display intense absorption maxima around 300 nm with extinction coefficients ranging from 30 900 to 60 400 $M^{-1}\,cm^{-1}$ (Table 2). Compounds **9a–d** additionally exhibit shoulders at 320 and 350 nm, while the longest wavelength absorption band appears with extinction coefficients

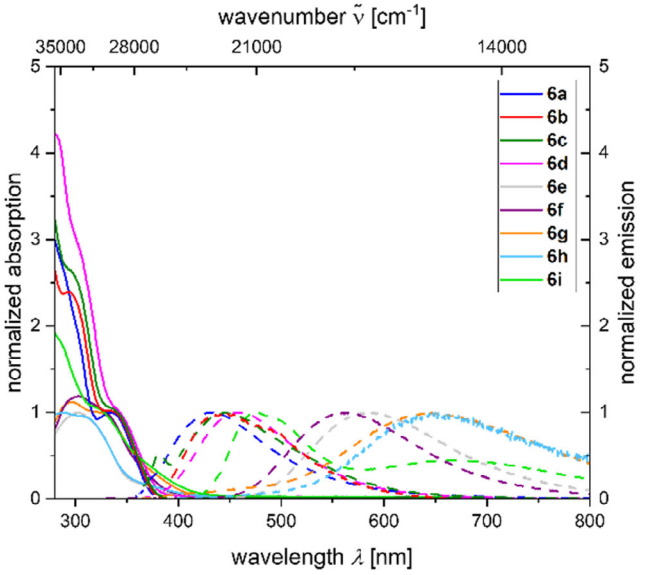

FIGURE 2 | Normalized UV/Vis absorption (recorded in CH_2Cl_2, $T = 293$ K, $c(\mathbf{6}) = 10^{-5}$ M, bold lines) and emission spectra (recorded in CH_2Cl_2, $T = 293$ K, $c(\mathbf{6}) = 10^{-5}$–10^{-6} M, dashed lines) of compounds **6**.

between 6700 and 11 200 $M^{-1}\,cm^{-1}$ (Figure 3). In contrast, the amino-substituted derivatives **9e** and **9f** show absorption maxima at 350 nm, with the longest wavelength absorption band appearing as a shoulder at 370 and 381 nm, respectively, and extinction coefficients of 22 400 and 27 300 $M^{-1}\,cm^{-1}$. In dichloromethane, dyes **9a–d** emit in a narrow range from 438 to 463 nm. However, dyes **9e** and **9f** display bathochromically shifted emission maxima at 510 and 550 nm with the highest fluorescence quantum yields Φ_F in solution, reaching up to 0.10. In the solid state, two trends are observed. Dyes **9a–d** emit at similar wavelengths as in solution with slightly higher quantum yields. For **9e** and **9f**, the emission maxima are hypsochromically shifted compared to solution. The highest fluorescence quantum yield Φ_F is observed for **9f** at 0.09. In direct comparison with previously reported donor–acceptor cruciform systems bearing the same substituent in the 8-position and an additional acceptor in 5-position [16], T-shaped psoralens display a slightly blueshifted absorption maxima, whereas the emission maxima remain within a comparable range.

In addition, derivatives **6f** and **9f** embedded in a PMMA (polymethyl methacrylate) matrix at 1 wt% were investigated. The aryl-substituted derivative **6f** exhibits an emission maximum at 469 nm with a fluorescence quantum yield Φ_F of 0.07, comparable to the one in the solid state (466 nm, 0.05). In contrast, the alkynylated derivative **9f** shows a pronounced hypochromic shift. In the PMMA film, the emission maximum is located at 466 nm (cf. 510 nm in the solid state), while the fluorescence quantum yield Φ_F increases from 0.09 in the solid state to 0.15 in the matrix. This behavior implies that the alkynylated derivatives **9** are considerably more sensitive to the polar environment of the PMMA matrix than the arylated derivatives **6** (for further details, see Supporting Information).

The longest wavelength absorption maxima $\lambda_{max,abs}$ of dyes **6a–e** and **6g** correlates well against the Hammett parameter σ_p ($\lambda_{max,abs} = 29\,335 + 1808\ \sigma_p$ [cm^{-1}], $r^2 = 0.91$). Considering derivatives **6a–e**, a strong correlation with the σ_{p+} ($r^2 = 0.93$) and the σ_R parameter (0.90) is also observed. In contrast, plotting $\lambda_{max,abs}$

TABLE 1 | Selected photophysical properties (absorption maxima in CH_2Cl_2 with absorption coefficients (ε) and emission maxima in CH_2Cl_2 and in the solid state with fluorescence quantum yields (Φ_F) and Stokes shifts ($\Delta\tilde{\nu}_s$)) of the compounds **6**.

Compound	$\lambda_{max,abs}$, nm[a] (ε, $M^{-1}cm^{-1}$)	$\lambda_{max,em(solution)}$[b], nm ($\Phi_F$)[c]	$\Delta\tilde{\nu}_s$, cm^{-1}[d]	$\lambda_{max,em(solid)}$, nm[e] (Φ_F)[c]
6a	271 (24 300), 334 (6900)	433 (<0.01)	6800	420 (0.02)
6b	294 (17 300), 339 (7200 sh)	447 (<0.01)	7100	425 (0.02)
6c	298 (10 900), 341 (4300 sh)	446 (<0.01)	6900	440 (0.03)
6d	281 (24 000), 343 (5300 sh)	458 (<0.01)	7300	449 (0.01)
6e	302 (19 100), 360 (3100 sh)	584 (0.03)	10 700	467 (0.10)
6f	303 (34 000), 330 (28 900 sh), 358 (12 900 sh)	556 (0.07)	9900	466 (0.05)
6g	298 (29 900), 323 (26 700 sh), 364 (11 400 sh)	643 (<0.01)	11 900	496 (0.14)
6h	300 (20 300), 375 (7000 sh)	646 (0.01)	11 200	529 (0.19)
6i	328 (8700), 370 (3500 sh)	476, 659 (0.01)	6000	554 (0.02)

[a]Recorded in CH_2Cl_2, $T = 293$ K, $c(\mathbf{6}) = 10^{-5}$ M.
[b]Recorded in CH_2Cl_2, $T = 293$ K, $c(\mathbf{6}) = 10^{-5}$–10^{-6} M.
[c]Absolute quantum yields determined with an integrating sphere.
[d] $\Delta\tilde{\nu}_s = \frac{1}{\lambda_{max,abs}} - \frac{1}{\lambda_{max,em}}$.
[e]Recorded at $T = 293$ K.

TABLE 2 | Selected photophysical properties (absorption maxima in CH_2Cl_2 with absorption coefficients (ε) and emission maxima in CH_2Cl_2 and in the solid state with fluorescence quantum yields (Φ_F) and Stokes shifts ($\Delta\tilde{\nu}_s$)) of the compounds **9**.

Compound	$\lambda_{max,abs}$, nm[a] (ε, $M^{-1}cm^{-1}$)	$\lambda_{max,em(solution)}$[b], nm ($\Phi_F$)[c]	$\Delta\tilde{\nu}_s$, cm^{-1}[d]	$\lambda_{max,em(solid)}$, nm[e] (Φ_F)[c]
9a	300 (39 500), 317 (33 500 sh), 348 (8300 sh)	427 (<0.01)	5300	438 (<0.01)
9b	296 (57 500), 314 (29 400 sh), 348 (6700 sh)	448 (<0.01)	6400	449 (0.01)
9c	296 (60 400), 317 (50 400 sh), 350 (11 200 sh)	442 (0.01)	5900	450 (0.04)
9d	300 (36 000), 322 (32 200 sh), 350 (8200 sh)	457 (0.01)	6700	463 (0.03)
9e	296 (30 900), 317 (31 200), 345 (32 700), 370 (22 400 sh)	586 (0.03)	10 000	550 (0.05)
9f	297 (36 200), 352 (31 400), 381 (27 300 sh)	551 (0.10)	8100	510 (0.09)

[a]Recorded in CH_2Cl_2, $T = 293$ K, $c(\mathbf{9}) = 10^{-5}$ M.
[b]Recorded in CH_2Cl_2, $T = 293$ K, $c(\mathbf{9}) = 10^{-5}$–10^{-6} M.
[c]Absolute quantum yields determined with an integrating sphere.
[d]$\Delta\tilde{\nu}_s = \frac{1}{\lambda_{max,abs}} - \frac{1}{\lambda_{max,em}}$.
[e]Recorded at $T = 293$ K.

of the alkynyl-substituted dyes **9a–e** against σ_p gives a poorer correlation ($\lambda_{max,abs} = 28\,507 + 1223\ \sigma_p$ [cm^{-1}], $r^2 = 0.68$). Similarly, correlations are found with the σ_{p+} ($r^2 = 0.75$) and σ_R ($r^2 = 0.74$) parameters. In contrast, σ_{p-} and σ_I parameters fail to show any significant correlation (for further information, see Supporting Information). The direct comparison of the slopes of the linear correlation underlines that the transmission of the electronic substituent effect through the triple bond is expectedly less effective. For both series, the linear Hammett correlation further manifests that increasing donor strength of the substituent leads to a bathochromic shift of the absorption maximum of the T-shaped dyes **6** and **9**, which very likely originates from the diminished energy gap of the frontier molecular orbitals.

2.3 | Solvatochromism

For the compounds **6f** and **9f**, a dependence of the emission maximum on solvent polarity was observed. The emission color changes upon eyesight from blue in toluene to red in acetonitrile (Figure 4). The emission solvatochromism for both derivatives was studied by absorption and emission spectroscopy in solvents of varying polarity to gain information about the polar nature of the excited state (for details on compound **6f**, see Supporting Information).

For compound **9f**, the absorption maxima are only slightly affected by solvent polarity; the longest wavelength absorption maximum appears within a narrow range of 373–378 nm. In contrast, the emission maxima exhibit pronounced positive solvatochromism, ranging from 454 to 612 nm (Figure 5). The appearance of single broad emission bands in solvents of different polarity, similar band shapes—in particular for the solvents toluene, EtOAc, THF, CH_2Cl_2, and acetone—and the absence of dual emission strongly account for a dipolar relaxation as the underlying mechanism of the observed emission solvatochromicity [20]. With increasing solvent polarity, the fluorescence quantum yield Φ_F decreases due to the energy gap rule [21].

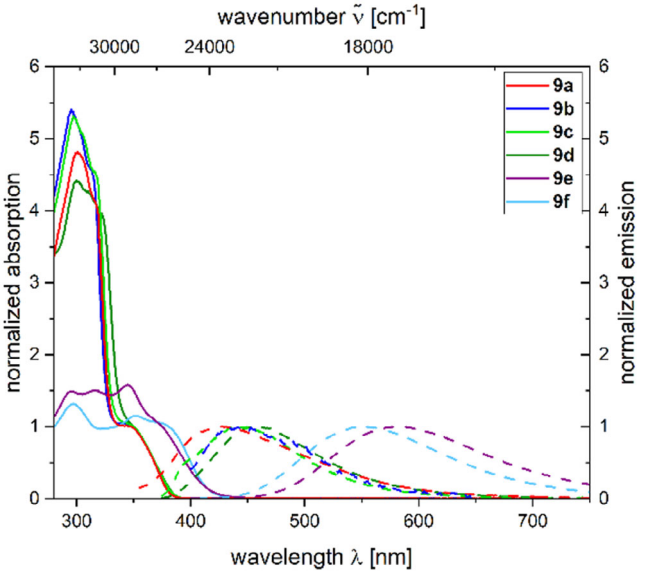

FIGURE 3 | Normalized UV/Vis absorption (recorded in CH_2Cl_2, $T = 293\ K$, $c(\mathbf{9}) = 10^{-5}$ M, bold lines) and emission spectra (recorded in CH_2Cl_2, $T = 293\ K$, $c(\mathbf{9}) = 10^{-5}$–10^{-6} M, dashed lines) of compounds **9**.

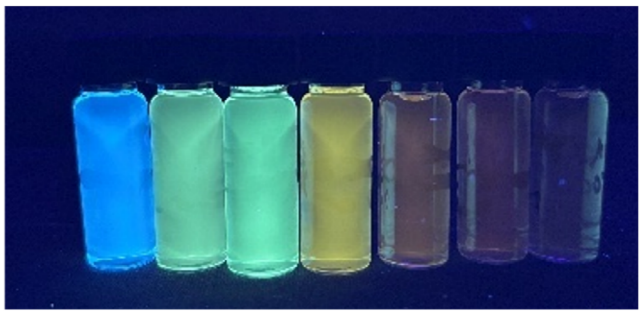

FIGURE 4 | Emission solvatochromism of compound **9f** (from left to right: toluene, EtOAc, THF, CH_2Cl_2, acetone, DMF, MeCN; $\lambda_{exc} = 365$ nm, $c(\mathbf{9f}) = 10^{-6}$ M).

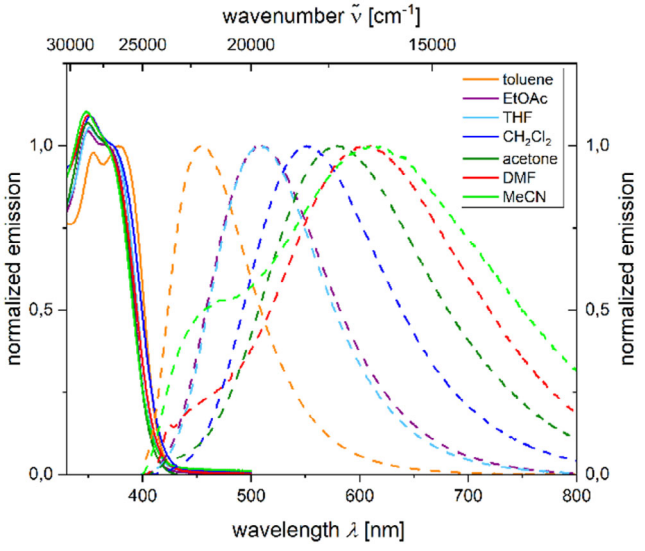

FIGURE 5 | UV/Vis absorption (bold lines) and emission (dashed lines) spectra of compound **9f** measured in seven different solvents.

TABLE 3 | UV/Vis absorption and emission maxima, absolute fluorescence quantum yields, and Stokes shifts of compound **9f** dependent on solvent polarity.

Solvent	$\lambda_{max,abs}$, nm[a] (ε, $M^{-1}\,cm^{-1}$)	$\lambda_{max,em}$, nm[b] (Φ_F)[c]	$\Delta\tilde{\nu}_s$, cm^{-1}
Toluene	298 (31 300), 355 (26 800), 378 (27 400)	454 (0.23)	4400
EtOAc	294 (32 600), 349 (30 700), 377 (27 400 sh)	510 (0.25)	6900
THF	296 (32 400), 352 (29 200), 373 (27 900 sh)	513 (0.30)	7300
CH_2Cl_2	297 (36 900), 352 (32 200), 381 (27 900 sh)	551 (0.10)	8100
Acetone	349 (29 000), 375 (25 400 sh)	580 (0.04)	9400
DMF	296 (31 400), 350 (28 600), 376 (24 700 sh)	606 (<0.01)	10 100
MeCN	294 (43 300), 348 (42 500), 377 (34 500 sh)	612 (0.01)	10 200

[a]Recorded in different solvents, $T = 293$ K, $c(\mathbf{9f}) = 10^{-5}$ M.
[b]Recorded in different solvents, $T = 293$ K, $c(\mathbf{9f}) = 10^{-6}$ M.
[c]Absolute quantum yields determined with an integrating sphere.

The highest fluorescence quantum yield is measured in THF at 0.30 (Table 3).

The observed emission solvatochromism is a consequence of the change of dipole moment of the fluorophore upon excitation by UV light and the associated dipole relaxation of the surrounding solvent molecules [20]. The change of the dipole moment $\Delta\mu$ can be quantified using the Lippert–Mataga model [22, 23]. First, the orientation polarizability Δf is determined according to Equation (1).

$$\Delta f = \frac{\varepsilon_r - 1}{2\varepsilon_r + 1} - \frac{n^2 - 1}{2n^2 + 1} \tag{1}$$

where ε_r is the relative permittivity and n is the refractive index of the respective solvents. The Lippert–Mataga equation (Equation (2)) can be used to calculate the change in dipole moment from the electronic ground state to the excited state.

$$\tilde{\nu}_a - \tilde{\nu}_f = \frac{2\Delta f}{4\pi\varepsilon_o hca^3}(\mu_E - \mu_G)^2 + \text{const.} \tag{2}$$

The two variables $\tilde{\nu}_a$ und $\tilde{\nu}_f$ define the absorption and emission maxima (in m^{-1}), ε describes the vacuum permittivity constant ($8.8542 \times 10^{-12}\ As\,V^{-1}\,m^{-1}$), h represents Planck's constant (6.2656×10^{-34} Js), and c the speed of light ($2.9979 \times 10^{8}\ ms^{-1}$). The variables μ_E and μ_G refer to the dipoles in the excited and ground states, while the variable α (in Å) describes the radius of the solvent cavity. Calculations for derivative **9f** were performed using the PBE1PBE [24, 25] functional and the 6-31G* [26, 27] basis set. In the gas phase, an Onsager radius of 6.01 Å was determined and for each solvent approximated based on the optimized ground state structure [28]. By plotting the Stokes shift $\Delta\tilde{\nu}_s$ against the orientation polarizability Δf, a change of dipole moment $\Delta\mu$ of 19.5 D (6.49×10^{-29} Cm) was determined with a goodness of fit ($r^2 = 0.96$). Dimethylformamide as a solvent was omitted in the

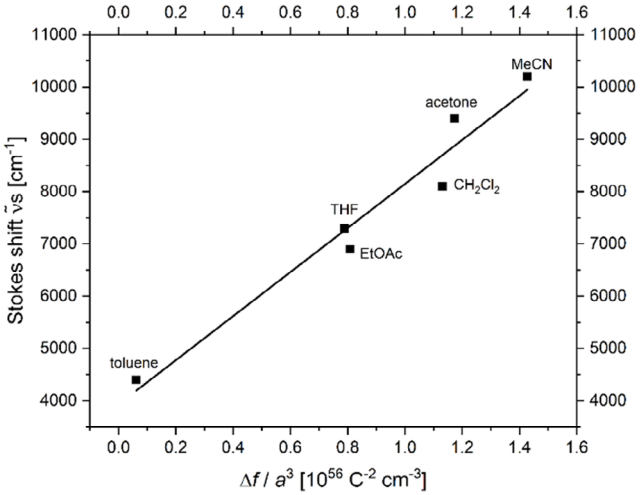

FIGURE 6 | Lippert plot for compound **9f** ($r^2 = 0.96$).

calculation (Figure 6). Likewise, a change of dipole moment of 18.8 D (6.26×10^{-29} Cm) was calculated for derivate **6f** (for further details, see Supporting Information). The results are comparable to those reported for a related, previously reported 8-(*p*-(dimethylamino)phenyl-substituted psoralen cruciform, where the positive solvatochromism amounts to a change of dipole moment of 17 D [16]. The increasing expansion of the π-system from the arylated to the alkynylated structure leads to an increase in the dipole moment change, which indicates an increase in the charge transfer character.

2.4 | Acidochromism

Protonation reveals another photophysical effect of derivative **6e**, which is evident in emission quenching upon addition of trifluoroacetic acid. This process can be reversed by adding triethylamine as a base (Figure 7).

The change in absorption can be quantified by recording absorption spectra by pH titration. Here, a decrease in the maxima at 235 and 271 nm can be observed, while there is an increase at 250.5 and 315 nm, which can be attributed to a species protonated on the dimethylamino group. Plotting the absorption intensities against the pH value leads to the determination of a pK_a value of 3.07, which is in good agreement with the value of 2.81 known from the literature for 5-dimethylaminophenyl-substituted 8-methoxypsoralen (for more details, see Supporting Information) [15].

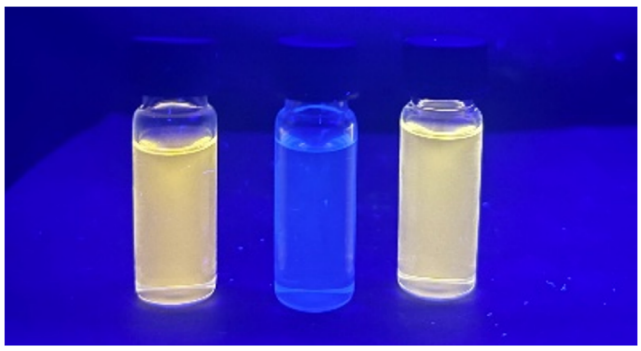

FIGURE 7 | Psoralen **6e** unprotonated (left), protonated with trifluoroacetic acid (center), and deprotonated with triethylamine (right) under UV-lamp ($\lambda_{exc} = 365$ nm, $c = 10^{-4}$ M).

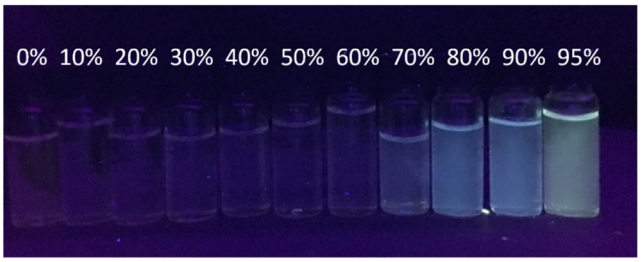

FIGURE 8 | Compound **6f** in different MeCN/H_2O mixtures ($\lambda_{exc} = 365$ nm, from left to right the ratio of water increases).

2.5 | Emission Upon Induced Aggregation

Some psoralen derivatives are highly emissive in solid state, whereas they are only weakly emissive in polar solvents. Compound **6f** was investigated on its aggregation-induced emission properties [29–32]. In pure acetonitrile, hardly any emission can be measured. Upon addition of water at constant psoralen concentration, an increase in fluorescence emission was observed (Figure 8). At a water content of 70%, the emission intensity increases significantly and remains nearly constant from 90% water. The emission maximum shifts bathochromically and is located at 493 nm in 90% water. At this solvent mixture, the emission intensity is approximately nine times higher than in pure acetonitrile (Figure 9).

2.6 | Calculated Electronic Structures

TD-DFT calculations were performed to obtain a deeper understanding of the electronic structures of the novel 8-substituted psoralen derivatives. The geometry of the optimized ground state and excited state was calculated using Gaussian 16 [33] with the PBE1PBE [24, 25] functional and the 6-31G* [26, 27] basis set. Since all photophysical measurements were performed in dichloromethane solution, the polarizable continuum model (PCM) with dichloromethane as the solvent was applied [34]. All minimum structures were verified by analytical frequency analysis. TD-DFT calculation for the dyes **6** and **9** was performed using the optimized S_0 geometries to reproduce the absorptions and the optimized S_1 geometries to describe the emission transitions. The experimental absorption and emission maxima of derivatives **6** and **9** are in good agreement with the computed values. The calculations indicate that the longest-wavelength absorption maxima of all derivatives can be attributed to HOMO→LUMO transitions. For the amino-substituted derivatives **6e**, **6f**, **9e** and **9f**, a better agreement between calculated and experimental emission maxima was obtained when the 6-311G basis set was employed (Table 4).

Within a substance class, the HOMO energies increase significantly with increasing donor strength. In contrast, the position of the LUMO is only slightly affected by the substituent pattern. As a result, the HOMO–LUMO energy gap decreases notably with increasing donor strength of the substituent in the 8-position,

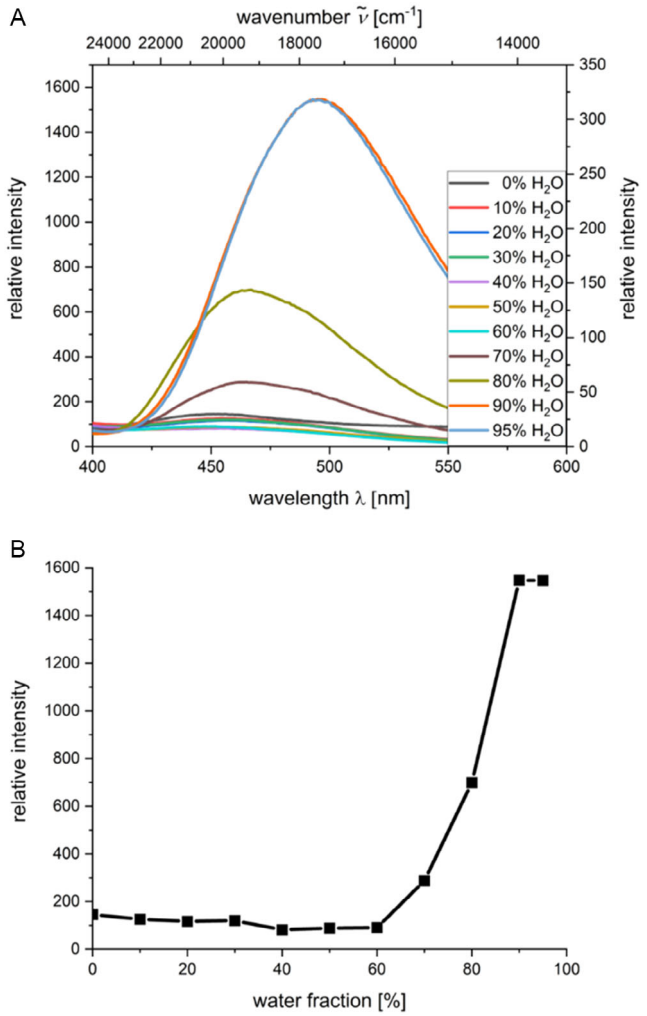

FIGURE 9 | (A) Emission spectra of compound **6f** in different MeCN/H_2O mixtures ($T = 293$ K, c(**6f**) $= 10^{-5}$ M, and $\lambda_{exc} = 300$ nm). (B) Change in emission intensity with the different water fractions.

which correlates with the experimentally observed bathochromic shift of the longest-wavelength absorption maximum. For identical substitution patterns, the HOMO energy of the alkynylated derivatives **9** is higher than that of the corresponding arylated derivative **6**. A similar trend is observed for the LUMO energies. However, the LUMO energies of the alkynylated derivatives are lower than those of the arylated analogs (Figure 10). The calculated frontier molecule orbitals of **6a, 9a**, **6d**, and **9d** indicate that the coefficient densities of the HOMOs are mainly located on the benzofuran ring and the substituent in 8-position. The LUMOs, however, predominantly localize coefficient density on the psoralen unit. For the compounds **6f** and **9f**, the coefficient densities of the HOMOs are preferentially localized on the amine substituent in 8-position. In contrast, in the LUMO, these are exclusively localized on the psoralen framework, confirming the pronounced charge–transfer character of these T-shaped chromophores and thereby explaining the strong emission solvatochromism. Compound **6f** is representative of the electronic structure of derivatives **6e–i**, which bear strong donor substituents and are characterized by HOMO energies between −5.324 and −5.006 eV as well as pronounced strong charge transfer properties (for further information, see Supporting Information).

3 | Conclusion

Starting from 8-methoxypsoralen, novel T-shaped psoralen derivatives bearing electron-deficient and electron-rich substituents at the 8-position were synthesized via Suzuki arylation and Sonogashira alkynylation. Expectedly, the absorption and emission properties strongly dependent on the substituent pattern. A bathochromic shift of the absorption and emission both in solution and in the solid state was observed with increasing donor strength of the substituents. The dependence of the absorption maximum on the electronic nature of the *para*-substituent correlates in a Hammett plot with σ parameters. The amino-substituted derivatives exhibit the longest wavelength absorption maxima at around 370 nm (i.e. close to the visible of the electronic spectrum). Furthermore, positive emission solvatochromism was detected and quantified according to Lippert–Mataga approach by determining the dipole moment change. The pK_a value of compound **6e** was determined from pH variation with absorption spectroscopy. TD-DFT calculations with the PBE1PBE functional are in good agreement with the experimental data, and the electronic structure of the longest wavelength absorption maximum could be elucidated. These findings are in line with our previous work on 5,8-disubstituted psoralen cruciform dyes. With bathochromically shifted absorption maxima, the amino-substituted derivatives represent promising candidates for application as PUVA reagents at excitation in the visible. The increased HOMO energies of amino-derivatives suggest that these dyes are more difficult to reduce, thereby favoring photoaddition with DNA over PET. Further investigation on the interaction of related chromophores with DNA are currently underway.

4 | Experimental Section

All experimental details, such as preparations of starting materials, typical procedures for the synthesis of compounds **6** and **9**, and all ^{1}H and ^{13}C NMR spectra, absorption and emission spectra, solvatochromism, and acidochromism as well as (TD) DFT calculations, are included in the Supporting Information.

4.1 | Typical Procedure for Synthesis of 8-Aryl-Psoralen Derivative (Compound 6a)

Under nitrogen in a Schlenk tube with magnetic stir bar, 8-triflato psoralen **4** (134 mg, 0.40 mmol, 1.00 equiv) was dissolved in dry THF (2.0 mL). Then, boronic acid ester **5a** (91 mg, 0.48 mmol, 1.20 equiv), potassium phosphate (340 mg, 1.60 mmol, 4.00 equiv), bis(dibenzylideneacetone)palladium(0) (46 mg, 0.08 mmol, 20 mol%), SPhos (41 mg, 0.10 mmol, 25 mol%), and water were added, and the solution was then degassed with nitrogen for 5 min. The reaction mixture was stirred for 24 h at 80°C (oil bath temperature). After cooling, deionized water (10 mL) was added and the aqueous phase was extracted with dichloromethane (3 ×30 mL). The combined organic phase was dried with anhydrous magnesium sulfate. The crude product was adsorbed on Celite and purified by column chromatography (*n*-hexane/ethyl acetate 1.5:1); compound **6a** (87 mg, 0.263 mmol, 66%) was isolated as a colorless solid. R_f (ethyl acetate/*n*-hexane 1:1.5): 0.44. Mp 229°C. ^{1}H NMR (300 MHz, $CDCl_3$): δ 6.42 (d, $J = 9.6$ Hz, 1H), 6.91 (d, $J = 2.3$ Hz, 1H), 7.74 (s, 1H), 7.71 (d, $J = 2.3$ Hz, 1H), 7.74 (s, 1H), 7.80 (d, $J = 8.3$ Hz,

TABLE 4 | Selected experimental and TD-DFT calculated absorption and emission maxima of compounds **6a-f** and **9a-f** (Gaussian 16, PBE1PBE/6-31G*).

Compound	$\lambda_{max,abs(exp)}$, nm[a] (ε, $M^{-1}\,cm^{-1}$)	$\lambda_{max,abs(calcd)}$, nm (oscillator strength), most dominant contribution	$\lambda_{max,em(exp)}$, nm[b]	$\lambda_{max,em(calcd)}$, nm (oscillator strength)[c]
6a	334 (6900)	328 (0.11), HOMO→LUMO (95%)	433	416 (0.16)
	271 (24 300)	287 (0.33), HOMO−1→LUMO (91%)		
6b	339 (7200 sh)	330 (0.09), HOMO→LUMO (96%)	447	423 (0.13)
	294 (17 300)	290 (0.32), HOMO−1→LUMO (92%)		
6c	341 (4300 sh)	334 (0.09), HOMO→LUMO (96%)	446	430 (0.13)
	298 (10 900)	294 (0.29), HOMO−1→LUMO (91%)		
6d	343 (5300 sh)	347 (0.09), HOMO→LUMO (95%)	458	452 (0.12)
	281 (24 000)	302 (0.20), HOMO−1→LUMO (90%)		
		274 (0.25), HOMO→LUMO+1 (81%)		
6e	360 (3100 sh)	406 (0.09), HOMO→LUMO (99%)	584	561 (0.08)[d]
	302 (19 100)	317 (0.99) HOMO−1→LUMO (72%)		
		308 (0.48), HOMO→LUMO+1 (76%)		
6f	358 (12 900 sh)	404 (0.13), HOMO→LUMO (98%)	556	535 (0.10)[d]
	330 (28 900 sh)	332 (0.49), HOMO→LUMO+1 (93%)		
	303 (34 000)	321 (0.14), HOMO−1→LUMO (92%)		
		307 (0.02), HOMO→LUMO+2 (95%)		
9a	348 (8300 sh)	351 (0.40), HOMO→LUMO (91%)	427	429 (0.38)
	317 (33 500 sh)	313 (0.63), HOMO−1→LUMO (42%)		
	300 (39 500)	299 (0.26), HOMO−1→LUMO (46%); HOMO→LUMO+1 (48%)		
9b	348 (6700 sh)	355 (0.30), HOMO→LUMO (68%)	448	440 (0.28)
	314 (29 400 sh)	309 (0.55), HOMO−1→LUMO (50%); HOMO → LUMO+1 (43%)		
	296 (57 500)			
9c	350 (11 200 sh)	360 (0.33), HOMO→LUMO (94%)	442	447 (0.30)
	317 (50 400 sh)	312 (0.59), HOMO−1→LUMO (43%); HOMO→LUMO+1 (47%)		
	296 (60 400)	300 (0.49), HOMO−1→LUMO (46%); HOMO → LUMO+1 (47%)		
9d	350 (8200 sh)	373 (0.34), HOMO→LUMO (95%)	457	466 (0.29)
	322 (32 200 sh)	317 (0.61), HOMO→LUMO+1 (61%)		
	300 (36 000)	305 (0.48), HOMO−1→LUMO (59%)		
9e	370 (22 400 sh)	422 (0.35), HOMO→LUMO (98%)	586	559 (0.19)[d]
	345 (32 700)	345 (0.83), HOMO→LUMO+1 (94%)		
	317 (31 200)	319 (0.19), HOMO−1→LUMO (88%)		
	296 (30 900)	288 (0.19), HOMO−2→LUMO (85%)		
9f	381 (27 300 sh)	424 (0.61), HOMO→LUMO (96%)	551	534 (0.28)[d]
	352 (31 400)	362 (0.62), HOMO→LUMO+1 (93%)		
		330 (0.16), HOMO−1→LUMO (84%)		
	297 (36 200)	311 (0.03), HOMO→LUMO+2 (94%)		
		298 (0.37), HOMO−2→LUMO (56%)		

[a]Recorded in CH_2Cl_2, $T = 293$ K, $c = 10^{-5}$ M.
[b]Recorded in CH_2Cl_2, $T = 293$ K, $c = 10^{-5}$–10^{-6} M.
[c]The most dominant contributions are HOMO → LUMO with a percentage of 98%–99%.
[d]Calculated with Gaussian 16, PBE1PBE/6-311G.

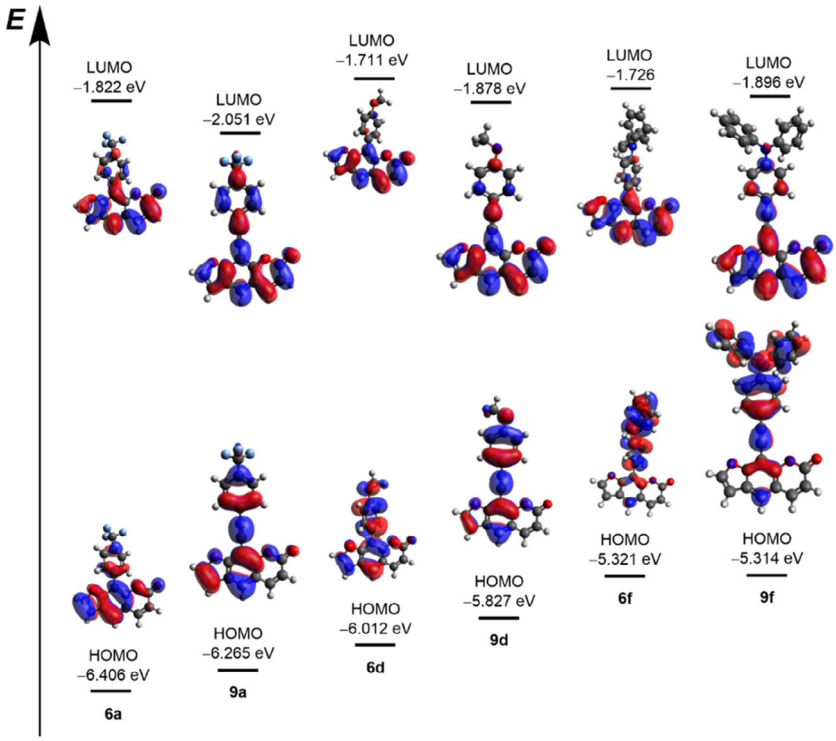

FIGURE 10 | Selected Kohn–Sham frontier molecular orbitals of compounds **6a**, **6d**, **6f**, **9a**, **9d**, and **9f** (PBE1PBE/6-31G*) and PCM with CH_2Cl_2 as solvent.

1H), 7.83–7.94 (m, 3H). ^{13}C NMR (75 MHz, $CDCl_3$): δ 106.9 (CH), 113.0 (C_{quat}), 114.9 (CH), 116.1 (C_{quat}), 119.9 (CH), 125.0 (C_{quat}), 125.5 (q, J_{CF} = 3.9 Hz, C_{quat}), 128.2 (q, J_{CF} = 319.5 Hz, C_{quat}), 130.7 (C_{quat}), 131.1 (CH), 144.5 (CH), 147.3 (CH), 148.5 (C_{quat}), 154.2 (C_{quat}), 160.6 (C_{quat}). MS (EI, m/z (%)): 331 (31), 330 ($[M]^+$, 100), 303 (23), 302 (91), 273 (14), 225 (14), 205 (34), 196 (11), 177 (16), 176 (55), 175 (17), 155 (12), 151 (20), 150 (10), 127 (17), 88 (24), 87 (14), 75 (16), 74 (10), 69 ($[CF_3]^+$, 23), 63 (10), 51 (13). IR $\tilde{\nu}$ [cm^{-1}]: 3129 (w), 3069 (w), 2922 (w), 2843 (w), 1717 (s), 1699 (m), 1667 (w), 1611 (m), 1591 (m), 1408 (m), 1393 (m), 1327 (s), 1290 (m), 1269 (m), 1223 (w), 1153 (m), 1113 (s), 1086 (m), 1069 (m), 1020 (m), 986 (m), 957 (w), 945 (w), 918 (m), 891 (m), 849 (s), 820 (m), 802 (w), 758 (s), 725 (m), 681 (m), 623 (m). Anal. calcd. for $C_{18}H_9F_3O_3$ [330.3]: C 65.46, H 2.75. Found: C 65.23, H 2.83.

4.2 | Typical Procedure for Synthesis of 8-Alkynyl-Psoralen Derivative (Compound 9a)

Under nitrogen in a Schlenk tube with magnetic stir bar, 8-triflato psoralen **4** (334 mg, 1.00 mmol, 1.00 equiv) was dissolved in dimethyl sulfoxide (4.5 mL). The acetylene **8a** (0.18 mL, 1.10 mmol, 1.10 equiv), triethylamine (0.21 mL, 1.51 mmol, 1.51 eq.), tetrakis(triphenylphosphane)-palladium(0) (23 mg, 0.020 mmol, 2.0 mol%), and copper iodide (7.6 mg, 0.040 mmol, 4.0 mol%) were added; the solution was then degassed with nitrogen for 5 min and stirred for 24 h at 90°C (oil bath temperature). After cooling, deionized water (10 mL) was added and the aqueous phase was extracted with dichloromethane (3 × 30 mL). The combined organic phases were dried with anhydrous magnesium sulfate, adsorbed on Celite, and purified by column chromatography (*n*-hexane/ethyl acetate 1.5:1). Compound **9a** (294 mg, 0.830 mmol, 83%) was isolated as a colorless solid. R_f (ethyl acetate/*n*-hexane 1:1): 0.62. Mp 180°C. ^{1}H NMR (300 MHz, $CDCl_3$): δ 6.44 (d, J = 9.5 Hz, 1H), 6.89 (d, J = 2.3 Hz, 1H), 7.58–7.71 (m, 3H), 7.75–7.89 (m, 4H). ^{13}C NMR (151 MHz, $CDCl_3$): δ 80.1 (C_{quat}), 97.0 (C_{quat}), 98.7 (C_{quat}), 107.0 (CH), 115.3 (CH), 115.7 (C_{quat}), 120.4 (CH), 124.0 (q, J_{CF} = 272.2, C_{quat}), 124.5 (C_{quat}), 125.4 (q, J = 3.6 Hz, CH), 130.7 (q, J = 32.7 Hz, C_{quat}), 132.4 (C_{quat}), 144.0 (CH), 147.4 (CH), 152.3 (C_{quat}), 156.5 (C_{quat}), 160.3 (C_{quat}). MS (EI, m/z (%)): 355 (26), 354 ($[M]^+$, 100), 335 ($[M\text{-}F]^+$, 7), 327 (17), 326 (74), 269 (13), 200 (16). IR $\tilde{\nu}$ (cm^{-1}): 3422 (w), 3292 (w), 3167 (w), 3121 (w), 3076 (w), 2374 (w), 1713 (s), 1605 (m), 1589 (m), 1539 (w), 1514 (w), 1425 (w), 1402 (m), 1342 (m), 1321 (s), 1294 (m), 1277 (w), 1238 (w), 1171 (m), 1125 (s), 1105 (s), 1067 (s), 1020 (m), 115 (m), 982 (m), 959 (m), 903 (m), 876 (m), 839 (s), 822 (m), 793 (w), 779 (m), 748 (m), 719 (m), 694 (w), 669 (w), 642 (m), 625 (w). Anal. calcd. for $C_{17}H_{10}O_3$ [262.1]: C 77.86, H 3.84. Found: C 77.95, 3.69.

Acknowledgments

We cordially thank the DFG (Mu 1088/9-1, Mu 1088/14-2) and the Fonds der Chemischen Industrie for financial support. Computational support and infrastructure were provided by the "Centre for Information and Media Technology" (ZIM) at the University of Düsseldorf. Thanks to the CeMSA@HHU (Center for Molecular and Structural Analytics @ Heinrich Heine University) for recording the mass-spectrometric and the NMR-spectroscopic data.

Open Access funding enabled and organized by Projekt DEAL.

Funding

This work was supported by the Deutsche Forschungsgemeinschaft (Mu 1088/9-1 and Mu 1088/14-2) and Fonds der Chemischen Industrie.

Conflicts of Interest

The authors declare no conflicts of interest.

Data Availability Statement

The data that support the findings of this study are available in the supplementary material of this article.

References

1. T. F. Anderson and J. J. Voorhees, "Psoralen Photochemotherapy of Cutaneous Disorders," *Annual Review of Pharmacology and Toxicology* 20 (1980): 235–257.

2. T. B. Fitzpatrick and M. A. Pathak, "Historical Aspects of Methoxsalen and other Furocoumarins," *Journal of Investigative Dermatology* 32 (1959): 229–231.

3. A. M. el-Mofty and M. M. Nada, "Vitiligo and its Treatment," *Australasian Journal of Dermatology* 15 (1974): 15–22.

4. A. M. el-Mofty, H. el-Sawalhy, and M. el-Mofty, "Clinical Study of a New Preparation of 8-methoxypsoralen in Photochemotherapy," *International Journal of Dermatology* 33 (1994): 588–592.

5. J. A. Parrish, T. B. Fitzpatrick, L. Tanenbaum, and M. A. Pathak, "Photochemotherapy of Psoriasis with Oral Methoxsalen and Longwave Ultraviolet Light," *New England Journal of Medicine* 291 (1974): 1207–1211.

6. E. A. Olsen, E. Hodak, T. Anderson, et al., "Guidelines for Phototherapy of mycosis fungoides and Sezary syndrome: A consensus statement of the United States Cutaneous Lymphoma Consortium," *Journal of the American Academy of Dermatology* 74 (2016): 27–58.

7. R. Edelson, C. Berger, F. Gasparro, et al., "Treatment of cutaneous T-cell lymphoma by extracorporeal photochemotherapy," *Preliminary results, New England Journal of Medicine* 316 (1987): 297–303.

8. T. C. Ling, T. H. Clayton, J. Crawley, et al., "British Association of Dermatologists and British Photodermatology Group Guidelines for the safe and Effective use of Psoralen-ultraviolet A Therapy 2015," *British Journal of Dermatology* 174 (2016): 24–55.

9. M. Zanolli, "Phototherapy Arsenal in the Treatment of Psoriasis," *Dermatologic Clinics* 22 (2004): 397–406.

10. A. Oroskar, G. Olack, M. J. Peak, and F. P. Gasparro, "4'-Aminomethyl-4,5',8-trimethylpsoralen Photochemistry: the Effect of Concentration and UVA Fluence on Photoadduct Formation in Poly(dA-dT) and Calf Thymus DNA," *Photochemistry and Photobiology* 60 (1994): 567–573.

11. N. Kitamura, S. Kohtani, and R. Nakagaki, "Molecular Aspects of Furocoumarin Reactions: Photophysics, Photochemistry, Photobiology, and Structural Analysis," *Journal of Photochemistry and Photobiology* 6 (2005): 168–185.

12. R. Johnson, L. Staiano-Coico, L. Austin, I. Cardinale, R. Nabeya-Tsukifuji, and J. G. Krueger, "PUVA treatment Selectively Induces a cell Cycle block and Subsequent Apoptosis in Human T-lymphocytes," *Photochemistry and Photobiology* 63 (1996): 566–571.

13. S. Fröbel, L. Levi, S. M. Ulamec, and P. Gilch, "Photoinduced Electron Transfer between Psoralens and DNA: Influence of DNA Sequence and Substitution," *ChemPhysChem* 17 (2016): 1377–1386.

14. S. Fröbel, A. Reiffers, C. Torres Ziegenbein, and P. Gilch, "DNA Intercalated Psoralen Undergoes Efficient Photoinduced Electron Transfer," *Journal of Physical Chemistry Letters* 6 (2015): 1260–1264.

15. S. R. Geenen, L. Presser, T. Hölzel, C. Ganter, and T. J. J. Müller, "Electronic Finetuning of 8-Methoxy Psoralens by Palladium-Catalyzed Coupling: Acidochromicity and Solvatochromicity," *Chemistry – A European Journal* 26 (2020): 8064–8075.

16. S. R. Geenen, T. Schumann, and T. J. J. Müller, "Fluorescent Donor-Acceptor Psoralen Cruciforms by Consecutive Suzuki-Suzuki and Sonogashira-Sonogashira One-Pot Syntheses," *Journal of Organic Chemistry* 85 (2020): 9737–9750.

17. B. L. Zhang, C. Q. Fan, L. Dong, F. D. Wang, and J. M. Yue, "Structural Modification of a Specific Antimicrobial Lead against Helicobacter Pylori Discovered from Traditional Chinese Medicine and a Structure–activity Relationship Study," *European Journal of Medicinal Chemistry* 45 (2010): 5258–5264.

18. J. M. Fevig, J. Feng, K. A. Rossi, et al., "Synthesis and SAR of 2,3,3a, 4-tetrahydro-1H-pyrrolo[3,4-c]isoquinolin-5(9bH)-ones as 5-HT2C Receptor Agonists," *Bioorganic & Medicinal Chemistry Letters* 23 (2013): 330–335.

19. A. Franz and T. Müller, "Facile Synthesis of Functionalized Oligophenothiazines via One-Pot Bromine-Lithium Exchange-Borylation-Suzuki Coupling (BLEBS)," *Synthesis* 2008 (2008): 1121–1125.

20. J. R. Lakowicz, *Principles of Fluorescence Spectroscopy*, 3rd ed. (Springer, 2006).

21. R. Englman and J. Jortner, "The Energy Gap Law for Radiationless Transitions in Large Molecules," *Molecular Physics* 18 (1970): 145–164.

22. E. Lippert, "Spektroskopische Bestimmung des Dipolmomentes aromatischer Verbindungen im ersten angeregten Singulettzustand," *Berichte der Bunsengesellschaft für Physikalische Chemie* 61 (2010): 962–975.

23. N. Mataga, Y. Kaifu, and M. Koizumi, "Solvent Effects upon Fluorescence Spectra and the Dipolemoments of Excited Molecules," *Bulletin of the Chemical Society of Japan* 29 (1956): 465–470.

24. C. Adamo and V. Barone, "Toward Reliable Density Functional Methods without Adjustable Parameters: The PBE0 Model," *Journal of Chemical Physics* 110 (1999): 6158–6170.

25. J. P. Perdew, K. Burke, and M. Ernzerhof, "Generalized Gradient Approximation Made Simple," *Physical Review Letters* 77 (1996): 3865–3868.

26. R. Krishnan, J. S. Binkley, R. Seeger, and J. A. Pople, "Self-Consistent Molecular-Orbital Methods .20. Basis Set for Correlated Wave-Functions," *Journal of Chemical Physics* 72 (1980): 650–654.

27. A. D. Mclean and G. S. Chandler, "Contracted Gaussian-Basis Sets for Molecular Calculations .1. 2nd Row Atoms, Z=11-18," *Journal of Chemical Physics* 72 (1980): 5639–5648.

28. L. Onsager, "Electric Moments of Molecules in Liquids," *Journal of the American Chemical Society* 58 (1936): 1486–1493.

29. Y. Hong, J. W. Lam, and B. Z. Tang, "Aggregation-induced Emission: Phenomenon, Mechanism and Applications," *Chemical Communications* 40 (2009): 4332–4353.

30. Y. Hong, J. W. Lam, and B. Z. Tang, "Aggregation-induced Emission," *Chemical Society Reviews* 40 (2011): 5361–5388.

31. R. Hu, N. L. Leung, and B. Z. Tang, "AIE macromolecules: syntheses, structures and functionalities," *Chemical Society Reviews* 43 (2014): 4494–4562.

32. J. Mei, N. L. Leung, R. T. Kwok, J. W. Lam, and B. Z. Tang, "Aggregation-Induced Emission: Together We Shine, United We Soar!," *Chemical Reviews* 115 (2015): 11718–11940.

33. M. J. Frisch, G. W. Trucks, H. B. Schlegel, G. E. Scuseria, et al. (Gaussian 16 Rev. C.01,2016): Wallingford, CT.

34. G. Scalmani and M. J. Frisch, "Continuous Surface charge Polarizable Continuum Models of Solvation. I. General Formalism," *Journal of Chemical Physics* 132 (2010): 114110.

35. M. Stephan, B. Stute, E. Lieres, and T. J. J. Müller, "Consecutive Three-Component Synthesis of Phenothiazine-Based Merocyanines – Bayesian Optimization, Electronic properties, and DSSC Characteristics," *European Journal of Organic Chemistry* 29 (2022): e202200163.

36. A. D. Buhimschi, D. M. Gooden, H. Jing, et al., "Psoralen Derivatives with Enhanced Potency," *Photochemistry and Photobiology* 96 (2020): 1014–1031.

37. C. Hansch, A. Leo, and R. W. Taft, "A Survey of Hammett Substituent Constants and Resonance and Field Parameters," *Chemical Reviews* 91 (1991): 165–195.

38. L. Mayer, L. May, and T. J. J. Müller, "The Interplay of Conformations and Electronic Properties in N-aryl Phenothiazines," *Organic Chemistry Frontiers* 7 (2020): 1206–1217.

39. C. Reichardt and T. Welton, *Solvents and Solvent Effects in Organic Chemistry*, 4th ed. (Wiley-VCH, 2010).

Supporting Information

Additional supporting information can be found online in the Supporting Information section. The authors have cited additional references within the Supporting Information [35–39]. **Supporting Fig. S1:** ^{1}H NMR spectrum of compound **4** ($CDCl_3$, 300 MHz, 298 K). **Supporting Fig. S2:** ^{13}C NMR spectrum of compound **4** ($CDCl_3$, 75 MHz, 298 K). **Supporting Fig. S3:** ^{1}H NMR spectrum of compound **6a** ($CDCl_3$, 300 MHz, 298 K). **Supporting Fig. S4:** ^{13}C NMR spectrum of compound **6a** ($CDCl_3$, 75 MHz, 298 K). **Supporting Fig. S5:** ^{1}H NMR spectrum of compound **6b** ($CDCl_3$, 600 MHz, 298 K). **Supporting Fig. S6:** ^{13}C NMR spectrum of compound **6b** ($CDCl_3$, 151 MHz, 298 K). **Supporting Fig. S7:** ^{1}H NMR spectrum of compound **6c** ($CDCl_3$, 600 MHz, 298 K). **Supporting Fig. S8:** ^{13}C NMR spectrum of compound **6c** ($CDCl_3$, 151 MHz, 298 K). **Supporting Fig. S9:** ^{1}H NMR spectrum of compound **6d** ($CDCl_3$, 600 MHz, 298 K). **Supporting Fig. S10:** ^{13}C NMR spectrum of compound **6d** ($CDCl_3$, 75 MHz, 298 K). **Supporting Fig. S11:** ^{1}H NMR spectrum of compound **6e** ($CDCl_3$, 300 MHz, 298 K). **Supporting Fig. S12:** ^{13}C NMR spectrum of compound **6e** ($CDCl_3$, 75 MHz, 298 K). **Supporting Fig. S13:** ^{1}H NMR spectrum of compound **6f** (DMSO-d_6, 300 MHz, 298 K). **Supporting Fig. S14:** ^{13}C NMR spectrum of compound **6f** (DMSO-d_6, 75 MHz, 298 K). **Supporting Fig. S15:** ^{1}H NMR spectrum of compound **6g** (DMSO-d_6, 300 MHz, 298 K). **Supporting Fig. S16:** ^{13}C NMR spectrum of compound **6g** ($CDCl_3$, 75 MHz, 298 K). **Supporting Fig. S17:** ^{1}H NMR spectrum of compound **6h** ($CDCl_3$, 300 MHz, 298 K). **Supporting Fig. S18:** ^{13}C NMR spectrum of compound **6h** ($CDCl_3$, 75 MHz, 298 K). **Supporting Fig. S19:** ^{1}H NMR spectrum of compound **6i** (acetone-d_6, 300 MHz, 298 K). **Supporting Fig. S20:** ^{13}C NMR spectrum of compound **6i** (acetone-d_6, 75 MHz, 298 K). **Supporting Fig. S21:** ^{1}H NMR spectrum of compound **9a** ($CDCl_3$, 300 MHz, 298 K). **Supporting Fig. S22:** ^{13}C NMR spectrum of compound **9a** ($CDCl_3$, 151 MHz, 298 K). **Supporting Fig. S23:** ^{1}H NMR spectrum of compound **9b** ($CDCl_3$, 300 MHz, 298 K). **Supporting Fig. S24:** ^{13}C NMR spectrum of compound **9b** ($CDCl_3$, 75 MHz, 298 K). **Supporting Fig. S25:** ^{1}H NMR spectrum of compound **9c** ($CDCl_3$, 300 MHz, 298 K). **Supporting Fig. S26:** ^{13}C NMR spectrum of compound **9c** ($CDCl_3$, 75 MHz, 298 K). **Supporting Fig. S27:** ^{1}H NMR spectrum of compound **9d** ($CDCl_3$, 300 MHz, 298 K). **Supporting Fig. S28:** ^{13}C NMR spectrum of compound **9d** ($CDCl_3$, 75 MHz, 298 K). **Supporting Fig. S29:** ^{1}H NMR spectrum of compound **9e** ($CDCl_3$, 300 MHz, 298 K). **Supporting Fig. S30:** ^{13}C NMR spectrum of compound **9e** ($CDCl_3$, 151 MHz, 298 K). **Supporting Fig. S31:** ^{1}H NMR spectrum of compound **9f** ($CDCl_3$, 300 MHz, 298 K). **Supporting Fig. S32:** ^{13}C NMR spectrum of compound **9f** ($CDCl_3$, 75 MHz, 298 K). **Supporting Fig. S33:** ^{1}H NMR spectrum of compound **6c** ($CDCl_3$, 600 MHz, 298 K). **Supporting Fig. S34:** ^{13}C NMR spectrum of compound **6c** ($CDCl_3$, 151 MHz, 298 K). **Supporting Fig. S35:** Recorded in dichloromethane, $\lambda_{ex} = \lambda_{max,abs}$, T = 293 K, c(**6a**) = 10^{-5}–10^{-6} M. **Supporting Fig. S36:** Recorded in dichloromethane, $\lambda_{ex} = \lambda_{max,abs}$, T = 293 K, c(**6b**) = 10^{-5}. **Supporting Fig. S37:** Recorded in dichloromethane, $\lambda_{ex} = \lambda_{max,abs}$, T = 293 K, c(**6c**) = 10^{-5}–10^{-6} M. **Supporting Fig. S38:** Recorded in dichloromethane, $\lambda_{ex} = \lambda_{max,abs}$, T = 293 K, c(**6d**) = 10^{-5}–10^{-6} M. **Supporting Fig. S39:** Recorded in dichloromethane, $\lambda_{ex} = \lambda_{max,abs}$, T = 293 K, c(**6e**) = 10^{-5}–10^{-6} M. **Supporting Fig. S40:** Recorded in dichloromethane, $\lambda_{ex} = \lambda_{max,abs}$, T = 293 K, c(**6f**) = 10^{-5}–10^{-6} M. **Supporting Fig. S41:** Recorded in dichloromethane, $\lambda_{ex} = \lambda_{max,abs}$, T = 293 K, c(**6g**) = 10^{-5}–10^{-6} M. **Supporting Fig. S42:** Recorded in dichloromethane, $\lambda_{ex} = \lambda_{max,abs}$, T = 293 K, c(**6h**) = 10^{-5}–10^{-6} M. **Supporting Fig. S43:** Recorded in dichloromethane, $\lambda_{ex} = \lambda_{max,abs}$, T = 293 K, c(**6i**) = 10^{-5}–10^{-6} M. **Supporting Fig. S44:** Recorded in dichloromethane, $\lambda_{ex} = \lambda_{max,abs}$, T = 293 K, c(**9a**) = 10^{-5}. **Supporting Fig. S45:** Recorded in dichloromethane, $\lambda_{ex} = \lambda_{max,abs}$, T = 293 K, c(**9b**) = 10^{-5}–10^{-6} M. **Supporting Fig. S46:** Recorded in dichloromethane, $\lambda_{ex} = \lambda_{max,abs}$, T = 293 K, c(**9c**) = 10^{-5}–10^{-6} M. **Supporting Fig. S47:** Recorded in dichloromethane, $\lambda_{ex} = \lambda_{max,abs}$, T = 293 K, c(**9d**) = 10^{-5}–10^{-6} M. **Supporting Fig. S48:** Recorded in dichloromethane, $\lambda_{ex} = \lambda_{max,abs}$, T = 293 K, c(**9e**) = 10^{-5}–10^{-6} M. **Supporting Fig. S49:** Recorded in dichloromethane, $\lambda_{ex} = \lambda_{max,abs}$, T = 293 K, c(**9f**) = 10^{-5}–10^{-6} M. **Supporting Fig. S50:** Solid state emission spectra recorded as powder, T = 293 K. **Supporting Fig. S51:** Solid-state emission spectra recorded as powder, T = 293 K. **Supporting Fig. S52:** Solid-state emission spectra recorded as powder, T = 293 K. **Supporting Fig. S53:** Solid-state emission spectra recorded as powder, T = 293 K. **Supporting Fig. S54:** Solid-state emission spectra recorded as powder, T = 293 K. **Supporting Fig. S55:** Solid-state emission spectra recorded as powder, T = 293 K. **Supporting Fig. S56:** Solid-state emission spectra recorded as powder, T = 293 K. **Supporting Fig. S57:** Solid-state emission spectra recorded as powder, T = 293 K. **Supporting Fig. S58:** Solid-state emission spectra recorded as powder, T = 293 K. **Supporting Fig. S59:** Solid-state emission spectra recorded as powder, T = 293 K. **Supporting Fig. S60:** Solid-state emission spectra recorded as powder, T = 293 K. **Supporting Fig. S61:** Solid-state emission spectra recorded as powder, T = 293 K. **Supporting Fig. S62:** Solid-state emission spectra recorded as powder, T = 293 K. **Supporting Fig. S63:** Solid-state emission spectra recorded as powder, T = 293 K. **Supporting Fig. S64:** Solid-state emission spectra recorded as powder, T = 293 K. **Supporting Fig. S65:** Emission spectra of 1 wt% PMMA film recorded at T = 293 K. **Supporting Fig. S66:** Emission spectra of 1 wt% PMMA film recorded at T = 293 K. **Supporting Fig. S67:** Hammett plot of absorption maxima $\lambda_{max,abs}$ [cm]$^{-1}$ against σ_p of psoralene **6a–e** and **6g** (recorded in CH_2Cl_2 at T = 298 K, c(**6**) = 10^{-5} M). **Supporting Fig. S68:** Hammett plot of absorption maxima $\lambda_{max,abs}$ [cm]$^{-1}$ against σ_{p+} of psoralene **6a–e** (recorded in CH_2Cl_2 at T = 298 K, c(**6**) = 10^{-5} M). **Supporting Fig. S69:** Hammett plot of absorption maxima $\lambda_{max,abs}$ [cm]$^{-1}$ against σ_{p-} of psoralene **6a–e** (recorded in CH_2Cl_2 at T = 298 K, c(**6**) = 10^{-5} M). **Supporting Fig. S70:** Hammett plot of absorption maxima $\lambda_{max,abs}$ [cm]$^{-1}$ against σ_R of psoralene **6a–e** (recorded in CH_2Cl_2 at T = 298 K, c(**6**) = 10^{-5} M). **Supporting Fig. S71:** Hammett plot of absorption maxima $\lambda_{max,abs}$ [cm]$^{-1}$ against σ_I of psoralene **6a–e** (recorded in CH_2Cl_2 at T = 298 K, c(**6**) = 10^{-5} M). **Supporting Fig. S72:** Hammett plot of absorption maxima $\lambda_{max,abs}$ [cm]$^{-1}$ against σ_p of psoralene **9a–e** (recorded in CH_2Cl_2 at T = 298 K, c(**9**) = 10^{-5} M). **Supporting Fig. S73:** Hammett plot of absorption maxima $\lambda_{max,abs}$ [cm]$^{-1}$ against σ_{p+} of psoralene **9a–e** (recorded in CH_2Cl_2 at T = 298 K, c(**9**) = 10^{-5} M). **Supporting Fig. S74:** Hammett plot of absorption maxima $\lambda_{max,abs}$ [cm]$^{-1}$ against σ_{p-} of psoralene **9a–e** (recorded in CH_2Cl_2 at T = 298 K, c(**9**) = 10^{-5} M). **Supporting Fig. S75:** Hammett plot of absorption maxima $\lambda_{max,abs}$ [cm]$^{-1}$ against σ_R of psoralene **9a–e** (recorded in CH_2Cl_2 at T = 298 K, c(**9**) = 10^{-5} M). **Supporting Fig. S76:** Hammett plot of absorption maxima $\lambda_{max,abs}$ [cm]$^{-1}$ against σ_I of psoralene **9a–e** (recorded in CH_2Cl_2 at T = 298 K, c(**9**) = 10^{-5} M). **Supporting Fig. S77:** UV/Vis absorption (bold lines) and emission (dashed lines) spectra of compound **6f** measured in six different solvents. **Supporting Fig. S78:** Lippert–Mataga plot for compound **6f** (r^2 = 0.90). **Supporting Fig. S79:** Lippert–Mataga plot for compound **9f** (r^2 = 0.96). **Supporting Fig. S80:** Absorption spectra of **6e** in the presence of increasing amounts of TFA (recorded in CH_2Cl_2, c(**6e**) = 2.3 · 10^{-5} M, T = 293 K. **Supporting Fig. S81:** Difference spectra for the absorption spectra of compound **6e** in the presence of increasing amounts of TFA (recorded in CH_2Cl_2, c(**6e**) = 2.3 · 10^{-5} M, T = 293 K. **Supporting Fig. S82:** Determination of the pK_a of **6e** by plotting the absorption intensity at 250.5 and 270 nm against pH-value. **Supporting Fig. S83:** Selected *Kohn–Sham* frontier molecular orbitals of compounds **6e–i** (PBE1PBE/6-31G*) and PCM with CH_2Cl_2 as solvent. **Supporting Table S1:** Experimental details for the synthesis of 8-aryl-psoralens **6**. **Supporting Table S2:** Experimental details for the synthesis of 8-alkynyl-psoralen derivatives **9**. **Supporting Table S3**: Tabular overview of utilized parameters.[37] **Supporting Table S4:** Solvent parameters and selected photophysical data and calculated Onsager radii of compound **6f**. **Supporting Table S5**: Solvent parameters and selected photophysical data and calculated Onsager radii of compound **9f**.